The Astrophysical Journal, 744:45 (9pp), 2012 January 1 doi:10.1088/0004-637X/744/1/45

MERGERS OF SUPERMASSIVE BLACK HOLES IN ASTROPHYSICAL ENVIRONMENTS

Tanja Bode[1], Tamara Bogdanović[2,3], Roland Haas[1], James Healy[1], Pablo Laguna[1], and Deirdre Shoemaker[1]
[1] Center for Relativistic Astrophysics and School of Physics, Georgia Institute of Technology, Atlanta, GA 30332, USA
[2] Department of Astronomy, University of Maryland, College Park, MD 20742, USA
Received 2011 January 24; accepted 2011 September 14; published 2011 December 13

ABSTRACT

Modeling the late inspiral and mergers of supermassive black holes (BHs) is central to understanding accretion processes and the conditions under which electromagnetic (EM) emission accompanies gravitational waves (GWs). We use fully general relativistic hydrodynamics simulations to investigate how EM signatures correlate with BH spins, mass ratios, and the gaseous environment in this final phase of binary evolution. In all scenarios, we find some form of characteristic EM variability whose detailed pattern depends on the spins and binary mass ratios. Binaries in hot accretion flows exhibit a flare followed by a sudden drop in luminosity associated with the plunge and merger, as well as quasi-periodic oscillations correlated with the GWs during the inspiral. Conversely, circumbinary disk systems are characterized by a low luminosity of variable emission, suggesting challenging prospects for their detection.

Key words: accretion, accretion disks – black hole physics – gravitational waves

Online-only material: color figures

1. INTRODUCTION

Gravitational waves (GWs) from the inspiral and coalescence of supermassive binary black holes (BBHs) contain detailed information about the black hole (BH) masses, their spins, and the orbital characteristics of the binary. Space-based GW observations will provide measurements of these quantities with a level of accuracy rarely attained by astronomical observations (Trias & Sintes 2008; Klein et al. 2009). Electromagnetic (EM) observations of these cataclysmic events, on the other hand, can provide an observational link between the merging BHs and their host galaxies by shedding light on the environment surrounding the holes and, in particular, by giving us insight about accretion and feedback processes. Our work investigates the circumstances under which detectable EM emission accompanies the GW signal from supermassive BBH mergers in astrophysical environments.

Our work complements non-relativistic hydrodynamic simulations that follow the inspiral of a supermassive BH pair in the aftermath of a galactic merger down to a scale of ∼0.01 pc. (see Colpi et al. 2007 for a review). These studies have provided clues about BH interactions with the surrounding stars and gas that lead to the formation of gravitationally bound binaries. They suggest that characteristic EM signatures may be associated with supermassive BBHs in this stage of evolution (Armitage & Natarajan 2002; Milosavljević & Phinney 2005; Dotti et al. 2006; Bogdanović et al. 2008, for example). Modeling at even smaller scales, where the orbital dynamics of the binary are determined by gravitational radiation, requires a post-Newtonian treatment of gravity and, in the last few tens of orbits and merger, the framework of general relativity. Examples of such works include recent numerical relativity studies of coalescing binaries surrounded by test particles (van Meter et al. 2010), gas (Bode et al. 2010; Farris et al. 2010), or EM fields (Palenzuela et al. 2009, 2010; Mösta et al. 2010).

Previously, in Bode et al. (2010), we carried out the first fully general relativistic hydrodynamics study of the late inspiral and merger of binaries with equal-mass and parallel-spin BHs in a hot accretion flow. This work together with Farris et al. (2010) established that the plunge and merger of "symmetric" binaries in hot accretion flows are characterized by an EM flare followed by a sudden drop-off in luminosity. Another of its findings is that the BBH orbital motion imprints a quasi-periodic signal in the light curve that is an EM equivalent of a GW chirp. However, it remained to be answered whether such signals are present for more generic binary configurations and in cooler accretion flows such as accretion disks. The present work investigates the effect of varying BH spins and mass ratios and considers astrophysically relevant environments that include circumbinary disks and hot, radiatively inefficient accretion flows (RIAFs). The hot flow and circumbinary disk effectively bracket a range of physical scenarios for a BBH environment characterized by the balance of heating and cooling processes in the gas. If cooling is more efficient, the gas settles into a rotationally supported accretion disk whereas when heating dominates it gives rise to a hot, tenuous, and geometrically thick accretion flow.

We consider binaries with BH masses m_i ($q = m_2/m_1 < 1$) and dimensionless spin parameters $\vec{a}_i/m_i$. The initial binary is on a quasi-circular orbit at a separation of $8\,M$ (in geometrical units), with $M = m_1 + m_2$ the total mass of the binary. We compute our results using M as a natural unit and present results scaled to a total mass of $10^7\,M_\odot$; that is, $M = 1.48 \times 10^{12}\,\mathrm{cm}\ M_7 = 49.4\,\mathrm{s}\ M_7$ with $M_7 = M/10^7\,M_\odot$. Since in all scenarios the mass of the gas in the vicinity of the binary is many orders of magnitude lower than M, the BBH dynamics is indistinguishable from the vacuum case. We use the computational methodology and infrastructure described in Bode et al. (2010), Ansorg et al. (2004), Baiotti et al. (2005), Cactus (2010), Einstein Toolkit (2010), Husa et al. (2006), Schnetter et al. (2004), and Thornburg (2004). Our simulations do not capture radiative transport, magnetic fields, or physical viscosity. Our computational grid had an outer boundary at $\sim 320\,M$, with 9 (10) levels of mesh refinement for the equal (unequal) BH mass binaries. Resolution at the finest level was $M/67(M/76)$, with subsequent levels increased by a factor of two. The 5 (7) finest levels had $42^3(36^3)$ grid points, while

[3] Einstein Postdoctoral Fellow.

the remaining ones had $84^3(72^3)$ grid points. A subset of runs at a higher resolution of $M/100$ showed that our results did not change significantly enough with resolution to affect our conclusions.

2. HOT ACCRETION FLOW

In this scenario, the BBH environment is assumed to have the properties of an RIAF. In RIAFs, most of the energy generated by accretion and turbulent stresses is stored as thermal energy in the gas, and the accretion flow is hot and geometrically thick (Ichimaru 1977; Narayan & Yi 1994). The electron and ion plasmas in RIAFs can form a two-temperature flow in which the thermal energy is stored in the ion plasma while the electron plasma cools more efficiently (i.e., $T_p \gtrsim T_e$). In such a case, the temperature of the plasma is represented by the ion temperature, while the characteristics of emitted radiation depend on the properties of electrons. The temperature ceiling reached by the ion plasma will be determined by cooling processes such as the thermal bremsstrahlung, synchrotron, and inverse Compton emission, as well as the electron–positron pair production and the pion decay resulting from energetic proton–proton collisions. Which process dominates the energy loss of the plasma sensitively depends on its density, temperature, and magnetic field strength, as well as the efficiency of coupling between ions and electrons. The latter process determines the rate with which energy can be transferred from hot ions to electrons, and consequently the ratio of their temperatures, $\varepsilon = T_e/T_p$. While modeling of the radiative cooling and treatment of the two-temperature plasma flow is beyond the capabilities of our code at this time, we capture the effect of different thermal properties of the plasma by investigating several initial ion plasma temperatures in our simulations, $T_p = \{10^{10}, 10^{11}, 10^{12}\}$ K. In order to evaluate the emission properties of these flows, we make a simplistic assumption that $\varepsilon = 10^{-2}$ everywhere in the accretion flow. This is an idealization as T_e/T_p is expected to vary in both space and time and can have a range of values between $\sim 10^{-2}$ and 0.1 depending on the dominant plasma processes (see, for example, Sharma et al. 2007). Our choice of ε is, however, conservative because it caps T_e and consequently the bremsstrahlung luminosity at lower values (see Section 2.2). The properties of the binary and initial T_p of the environment are listed in the top part of Table 1.

Table 1
Parameters for Scenarios Discussed for Hot Accretion Flows and Circumbinary Disks

Case	q	$\vec{a}_1/m_1$	$\vec{a}_2/m_2$	T_p (K)
Hot Accretion Flows				
CH1	1	(0, 0, 0.6)	(0, 0, 0.6)	10^{12}
CM1	1	(0, 0, 0.6)	(0, 0, 0.6)	10^{11}
CL1	1	(0, 0, 0.6)	(0, 0, 0.6)	10^{10}
CH2	1/2	(0, 0, 0.6)	(0, 0, 0.6)	10^{12}
CH3	1/2	(−0.40, 0.44, −0.02)	(−0.16, 0.54, −0.21)	10^{12}
CH4	1/2	(−0.35, −0.47, 0.10)	(0.28, 0.44, 0.30)	10^{12}
Circumbinary Disks				h/r
DA1	1	(0, 0, 0.6)	(0, 0, 0.6)	0.2
DB1	1	(0, 0, 0.6)	(0, 0, 0.6)	0.4
DC1 *	1	(0, 0, 0.6)	(0, 0, 0.6)	0.2
DA2	1/2	(0, 0, 0.6)	(0, 0, 0.6)	0.2
DA3	1/2	(−0.40, 0.44, −0.02)	(−0.16, 0.54, −0.21)	0.2
DA4	1/2	(−0.35, −0.47, 0.10)	(0.28, 0.44, 0.30)	0.2

Notes. The central columns describe the black hole parameters of the system while the last column designates the primary parameter for the initial gas configuration. The "∗" refers to retrograde circumbinary disk rotation.

2.1. Initial Conditions

The gas around the binary is initialized with uniform density and temperature and modeled with a polytropic index $\gamma = 5/3$, adequate for the ion plasma which is non-relativistic at temperatures $T_p \lesssim 10^{12}$ K ($kT_p \lesssim 100$ MeV). The gas initially has zero linear and angular momentum. The latter condition is consistent with the expectations based on the self-similar solutions for RIAFs described by Narayan & Yi (1994) for $\gamma = 5/3$ gas. This initial configuration is first evolved on the static BBH spacetime for the duration of 32 M and subsequently on a dynamic BBH spacetime for 160 M.[4] In comparison, the relaxation time of the gas within the Bondi radius of the gravitational influence of the binary ($t_{\rm relax} = R_{\rm B}/c_s$, where c_s is the speed of sound) is 18 M, 530 M, and 1.7×10^4 M for 10^{12} K, 10^{11} K and 10^{10} K gas, respectively. Longer relaxation timescales for 10^{10} K and 10^{11} K gas imply that at the beginning of the simulation the gas is still settling into a quasi-hydrostatic equilibrium and flowing toward the center of the potential. We verified for all simulations that relaxation is a gradual process which can be reproduced in simulations of accretion flows with the same properties surrounding a single BH with a mass equal to that of the BBH. We use the fact that the relaxation process does not introduce rapid transients (i.e., on the BBH orbital timescale) in the light curve of either system to remove a smooth secular modulation in luminosity amplitude caused by relaxation by dividing a light curve calculated for the BBH system by its single BH equivalent. Using this ansatz we disentangle the effects of the gas relaxation from variability driven by the orbiting BBH while at the same time reducing the computational expense of our simulations to about 800 M per simulation. This computational gain ultimately allows us to explore a relatively wide parameter space of the BBHs and gas in this work.

2.2. Properties of the Accretion Flow

In all models, a pair of denser gas wakes quickly forms behind the orbiting holes after the beginning of the simulation. About two orbits before merger, a high-density, dynamically unstable region is also formed inside the binary orbit. After coalescence, this structure is promptly swallowed by the newly formed BH. Both the wakes and the high-density central region are associated with strong shocks, driven by the orbiting BBH, and their evolution gives rise to the characteristic variability of the emitted light. This is illustrated in the top panels of Figure 1, which show bremsstrahlung luminosity as a function of time, integrated within the sphere of radius $R = 20\,M$ and normalized by the light curve for a single BH with equivalent mass. We verified that variability in the accretion flow associated with the BBH evolution is enclosed within this volume by varying our choice of R and confirmed that the central region contributes the dominant component of the luminosity to the light curve of the binary.

The top left panel in Figure 1 shows a broad peak in luminosity whose growth coincides with the formation of the shocked region within the binary orbit. As the binary shrinks, the brightness of this region increases until the merger at which point the final BH swallows the shocked gas and the luminosity

[4] To ensure that this initial phase of relaxation does not introduce spurious transients to our analysis, we omit it and only report the subsequent evolution.

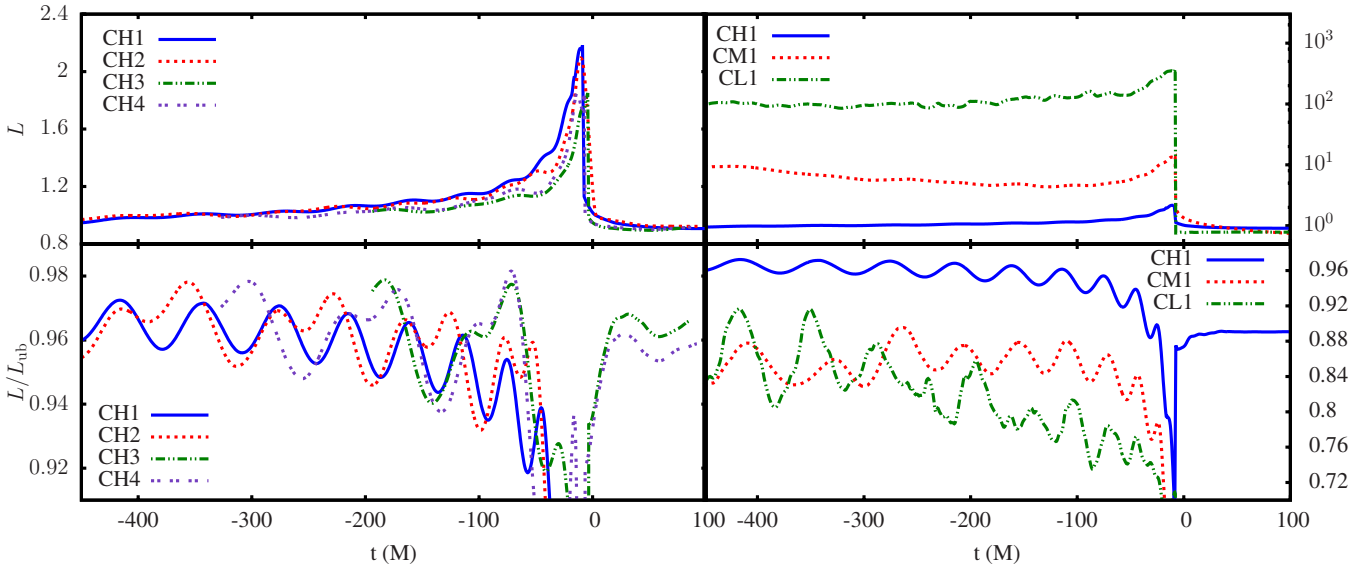

Figure 1. Top: bremsstrahlung luminosity in hot accretion flows for different BBH configurations (left) and accretion flow temperatures (right) normalized to the luminosity of a single BH with corresponding mass. Bottom: ratio of beamed to unbeamed luminosity $L_{\rm ub}$ for different BBH configurations (left) and different accretion flow temperatures (right) for an observer viewing the binary edge-on. Coalescence occurs at $t = 0$.

(A color version of this figure is available in the online journal.)

precipitously drops off. The top left panel of Figure 1 compares the light curves calculated for different BBH configurations in an environment with an initial temperature $T_p \approx 10^{12}$ K. The $q = 1/2$ case (CH2) exhibits a lower and narrower luminosity peak relative to the $q = 1$ case (CH1). This is because orbital torques from an unequal-mass binary are less efficient at driving shocks in the gas, resulting in a less luminous and delayed emission from this region. In $q = 1/2$ systems with generic spin orientations (CH3 and CH4), the luminosity peaks at even lower values, at ∼80% of the amplitude achieved by the $q = 1$ binary. This is a consequence of the orbital precession present in binaries with misaligned spins, which further inhibits the formation of a stable shock region between the holes. The gradual rise and sudden drop-off in luminosity, however, seem to be *a generic feature of all modeled light curves, regardless of the spin configuration and the mass ratios* explored in our simulations. Moreover, the same feature has been observed for a wide range of initial conditions employed in previous works carried out by our group (Bode et al. 2010) and by other authors (Farris et al. 2010), indicating that this is a robust signature of binary systems merging in hot accretion flows.

To understand the dependence of the luminosity on the properties of the system, we estimate the bremsstrahlung luminosity emitted from the Bondi radius of gravitational influence, $R_{\rm B} \approx 6.5\, M\, T_{p,12}^{-1}$, as

$$L_{\rm brem} \approx 6.7 \times 10^{40}\,{\rm erg\,s^{-1}}\,\varepsilon_{-2}^{1/2}\,T_{p,12}^{-1/2} \times (1 + 4.4\,\varepsilon_{-2}\,T_{p,12})_{5.4}\,\tau_T^2\,M_7^4\,, \quad (1)$$

where $\varepsilon = 10^{-2}\varepsilon_{-2}$, $T_p = 10^{12}\,{\rm K}\,T_{p,12}$, $\tau_T = \sigma_{\rm T}\,\rho\,R_{\rm B}$ is the optical depth of Thomson scattering within the Bondi sphere, $\sigma_{\rm T}$ is the cross-section of Thomson scattering, and ρ is the gas density. The subscript "5.4" indicates that the expression in the brackets is normalized to this value. Note that Equation (1) implies *a maximum* bremsstrahlung luminosity that can be reached by an accretion flow as long as its optical depth $\tau_{\rm T} \lesssim 1$ (we consider Thomson scattering to be the dominant source of opacity in this regime). Flow with a larger optical depth would be subject to radiation pressure which could alter the kinematics of the gas or unbind it from the BBH altogether, thus acting to erase the variability imprinted by the binary motion and suppress the luminosity.

The top right panel in Figure 1 shows the light curves calculated for parallel-spin $q = 1$ binaries in gas with initial temperatures $T_p = \{10^{10}, 10^{11}, 10^{12}\}$ K. Lower temperature flows tend to exhibit a larger luminosity peak and a more dramatic drop-off than the hotter flows. This is because in colder flows the shocks can be very effectively excited by the merging binary. We find that regardless of its initial temperature, the gas in the vicinity of the holes is persistently shock-heated to a temperature ∼10^{12} K as a consequence of the binary orbital motion. Hence, the height of the peaks in the top right panel of Figure 1 reflects the ratio of bremsstrahlung emissivities of the gas in the BBH system ($T_p \approx 10^{12}$ K) to that in the single BH system ($T_p \approx \{10^{10}, 10^{11}, 10^{12}\}$ K), where bremsstrahlung emissivity $\propto T_p^{1/2}(1 + 4.4\,\varepsilon_{-2}\,T_{p,12})$. It follows from this simple estimate that the relative height of the BBH luminosity peak is 54, 12, and 1, respectively, consistent within a factor of a few with the values that we calculate from simulations.

If the hot accretion flow is threaded by a strong magnetic field, a significant fraction of its luminosity could be emitted in the form of synchrotron radiation which, assuming field strength $B = 10^4\,G\,\beta_{10}^{-1/2}\,T_{p,12}\,\tau_T^{1/2}\,M_7^{-1/2}$, could reach

$$L_{\rm syn} \approx 4 \times 10^{42}\,{\rm erg\,s^{-1}}\,\beta_{10}^{-1}\,\tau_T^2\,M_7^4\,, \quad (2)$$

where $\beta = 8\pi p_{\rm th}/B^2 = 10\,\beta_{10}$ is the ratio of thermal to magnetic pressure in the gas, expected to reach values of 1–10 in the central regions of RIAFs (Cao 2011). The presence of the softer photons supplied in situ by synchrotron and bremsstrahlung emission would also give rise to the inverse Compton radiation of similar magnitude:

$$L_{\rm IC} \approx 2\,L_{\rm soft}\,T_{p,12}^{-2}\,\tau_T\,M_7^3\,, \quad (3)$$

where relativistic factors have been evaluated for $v/c \approx 0.3$, appropriate for the BBH regime close to the merger, and $L_{\rm soft}$ is the luminosity of soft radiation.

Where the high energy tail of protons reaches the threshold of $kT_p = 100$ MeV an additional high energy process contributes to the radiative cooling: proton–proton collisions result in copious pion production, followed by pion decay to two γ-ray photons, $p + p \rightarrow p + p + \pi^0 \rightarrow p + p + 2\gamma$ (Dahlbacka et al. 1974; Eilek & Kafatos 1983; Colpi et al. 1986; Mahadevan et al. 1997; Oka & Manmoto 2003; Bhattacharyya et al. 2006). Following Colpi et al. (1986), who calculated the γ-ray emission from the p–p collisions of a thermal distribution of protons in the vicinity of a single Kerr BH, we estimate

$$L_{pp} \approx 2\text{–}13 \times 10^{39}\,\mathrm{erg\,s^{-1}}\; T_{p,12}\; \tau_T^2\; M_7\,, \qquad (4)$$

where the two extreme values correspond to a static and maximally rotating BH, respectively. We expect the luminosity in the BBH system to be closer to the higher value because the gas in the rotating and dynamic spacetime of the pair of orbiting BHs is very efficiently shock-heated to 100 MeV. The emission of γ-rays due to the pion decay is strongly suppressed in the limit $\tau_T \gtrsim 1$ due to the increased cross-section of γ-ray photons to electron–positron pair production, as well as the increased coupling between electron and proton plasma, which lowers T_p below the energy threshold for pion production (Colpi et al. 1986). In calculating luminosities in this section, we assumed the gas to be optically thin within the Bondi radius, which sets *an upper limit* on the gas density of the hot accretion flow, and thus $L_{\rm brem}$, $L_{\rm syn}$, $L_{\rm IC}$, and $L_{\rm pp}$.

The spectral energy distribution of these sources would be similar to a group of low-luminosity active galactic nuclei (AGNs) to which RIAF models have been applied (see Nemmen et al. 2006, for example). Spectral bands where these emission mechanisms are expected to peak in the reference frame of the binary are submillimeter (synchrotron), UV/X-ray (inverse Compton), ∼1 MeV γ-ray (bremsstrahlung and inverse Compton), and ∼20 MeV (pion decay). Additional components that we do not model in this work but which could also arise and in principle overtake the emission from the hot gas are the wide-band non-thermal synchrotron emission, if active and persistent jets are present in the system, as well as the optical/UV emission associated with the accretion disk that may encompass the hot flow at larger radii (Ho 2005).

The bottom panels in Figure 1 focus on oscillations in luminosity due to relativistic beaming and Doppler boosting of light emitted by the gas wakes. We account for these effects by multiplying the broadband emissivity of the gas (i.e., the luminosity per unit volume) by a factor $\{W[1-\beta\cos(\theta)]\}^{-4}$ and integrate over the volume to obtain the bolometric luminosity. Here, W is the local Lorentz factor and $\beta\cos(\theta)$ is the projection of the local three-velocity to the line of sight of the observer. We do not account for the bending of light and gravitational redshift of photons in the potential well of the BBH. The variations in luminosity shown in Figure 1 are calculated for a distant observer placed in the plane of the binary at infinity, an orientation for which the oscillations in the light curve are maximized. To emphasize the oscillations, the bottom panels show the ratio of beamed to unbeamed light curves. The most notable difference among simulated binary configurations is that the $q = 1$ case (CH1) yields sinusoidal oscillations, while the $q = 1/2$ cases (CH2, CH3, and CH4) give rise to double-peaked oscillations. We also find that in configurations with arbitrary spin orientation (CH3 and CH4) the sinusoidal peaks exhibit the largest degree of asymmetry. This is because the binary with parallel spins (CH2) stirs the surrounding gas more uniformly than binaries with misaligned spins (CH3 and CH4), which precess about the original orbital plane.

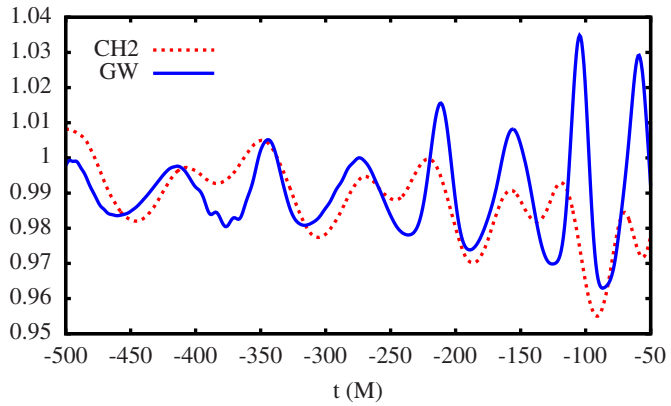

Figure 2. Beamed to unbeamed light curve ratio from case CH2 in Figure 1 and the corresponding GW in arbitrary units.

(A color version of this figure is available in the online journal.)

The bottom right panel illustrates the dependence of the oscillations on temperature. The most prominent oscillations are again associated with the lower temperature flow, which is more susceptible to shocking by the binary. While the high temperature of the gas in the CH1 case prevents formation of the strong density gradients, the lower temperature flows allow the density wakes to interact and waves of gas to propagate within the inner region, giving rise to more varied features in the oscillations. In all cases, the oscillations in luminosity are mirrored by the GWs. Figure 2 shows how the double-peaked structure in case CH2 emerges in both the luminosity and the GWs when the binary is observed edge-on. The double peaks in the GWs arise from the superposition of $l = 2$ and $l = 3$ modes in $q \neq 1$ binaries.

Figure 3 shows how oscillations vary as a function of inclination. The light curves have been evaluated for the $q = 1$ binary for three different temperature cases (CH1, CM1, and CL1) and the inclination angle is defined with respect to the initial binary orbital plane. Here again we show the ratio of beamed to unbeamed light curves. Because the motion of the denser gas wakes is tied to the plane of the binary, the oscillations in all runs disappear with increasing inclination angle. The relative drop in the luminosity of beamed light just prior to the coalescence is a consequence of the de-boosting of light caused by the strong radial inflow of the gas toward the BHs in this final stage of their evolution. The most notable difference among the three runs is that the oscillation curves exhibit more structure with decreasing temperature. This can be understood because the lower temperature gas is more clumpy and more prone to shocks, while in high-temperature flows, higher thermal velocity of the gas acts to erase density inhomogeneities. Along similar lines, lower temperature gas has less pressure support against infall, leading to higher infall velocities and thus more significant de-boosting with respect to the unbeamed luminosity case. In the precessing binaries, the time-varying inclination of the orbital plane imposes an additional modulation of the oscillations. Of the situations considered in this paper, two generic BBH systems, CH3 and CH4, precess due to their misaligned spins. The maximum precession angle attained over the entire evolution is at most 13° with respect to the initial orientation of the orbital plane, resulting in only minor modulation in their light curves.

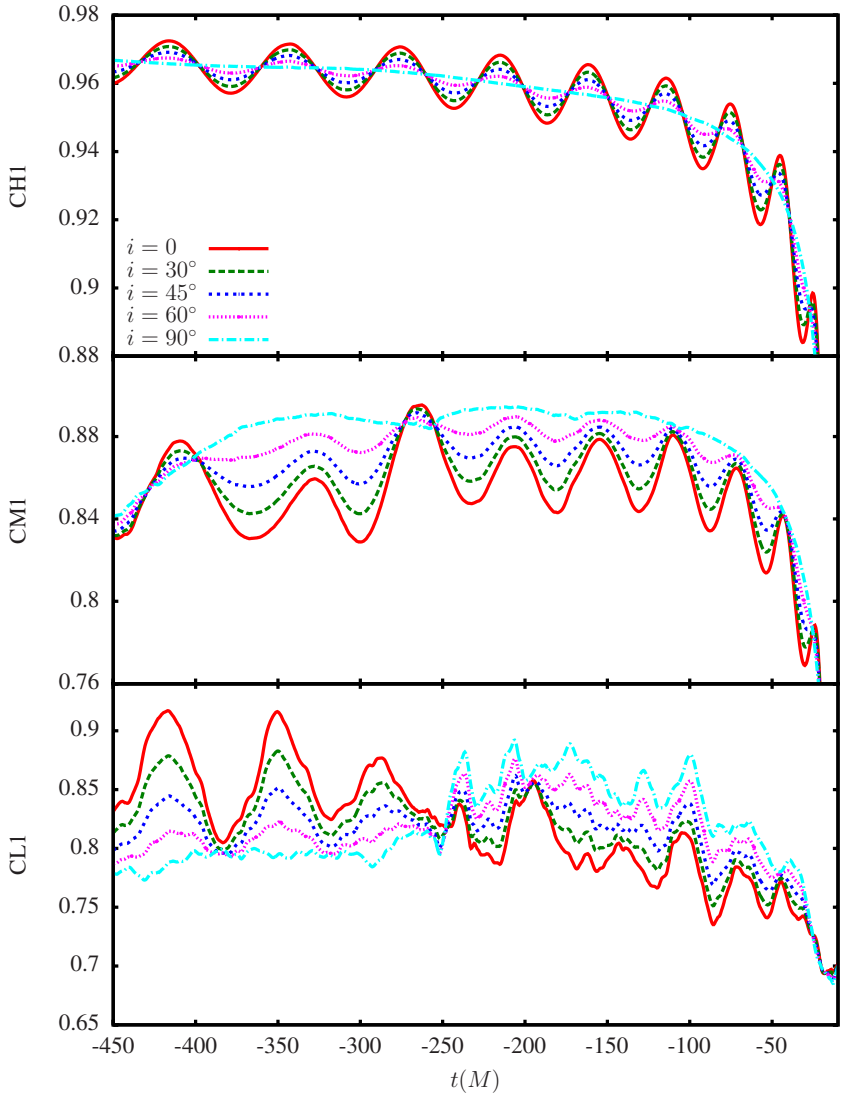

Figure 3. Variation of the bremsstrahlung luminosity oscillations with inclination angle i in accretion flows of initial proton temperature 10^{12}, 10^{11}, and 10^{10} K from top to bottom, respectively.

(A color version of this figure is available in the online journal.)

It is worth noting that accounting for the effects of light bending and gravitational redshift would result in the modified variability pattern of emitted light, relative to those shown in Figure 3. The photons most strongly affected by the general relativistic effects are emitted by the gas wake associated with the "background" BH, as seen from the perspective of an observer. This is because these photons travel across the deepest part of the potential well of the binary before escaping to infinity. However, most of the boosted light contributing to the peaks in the oscillations is emitted by the foreground wake, associated with the BH moving toward the observer and thus with photons which escape from the perimeter of the BBH orbit without crossing the deepest part of its potential well. These photons will be less affected by the general relativistic effects, thus partly justifying our simplistic approach to calculating the light curves.

3. CIRCUMBINARY DISKS

3.1. Initial Conditions

In this scenario, we consider circumbinary disks whose inner edge, the location where the torques from the binary are expected to create a low-density "hole" in the disk center (Artymowicz & Lubow 1994), is set at $r = 16\,M$. This choice is motivated by the requirement that the inner edge of the disk "follows" the shrinkage of the binary and remains at twice its semimajor axis until a binary separation of $8\,M$. In the context of the Shakura & Sunyaev (1973) model of a steady-state accretion disk, this requirement translates into the value of the half-thickness ratio of the disk, h/r, when the rate of viscous inflow of the disk, $\dot{a}_{\rm visc} = -1.5\,(h/r)^2\,\alpha\,V_K$, is set equal to the inspiral rate of the binary from gravitational radiation losses (Peters 1964). Here, V_K is the Keplerian velocity at the inner disk edge. This equality is satisfied for $h/r = 0.2$ (0.4) and a viscosity coefficient $\alpha = 0.4$ (0.1). Note that there are uncertainties associated with this estimate since the steady-state model does not fully capture the dynamics of the disk close to the BH coalescence. We follow O'Neill et al. (2009) and set up gas-pressure-supported disks characterized by a constant midplane density and entirely azimuthal initial gas velocities.

As in the case of hot accretion flows, here we only consider BBHs on quasi-circular orbits. This is based on the expectation that late in the BBH inspiral any initial orbital eccentricity will

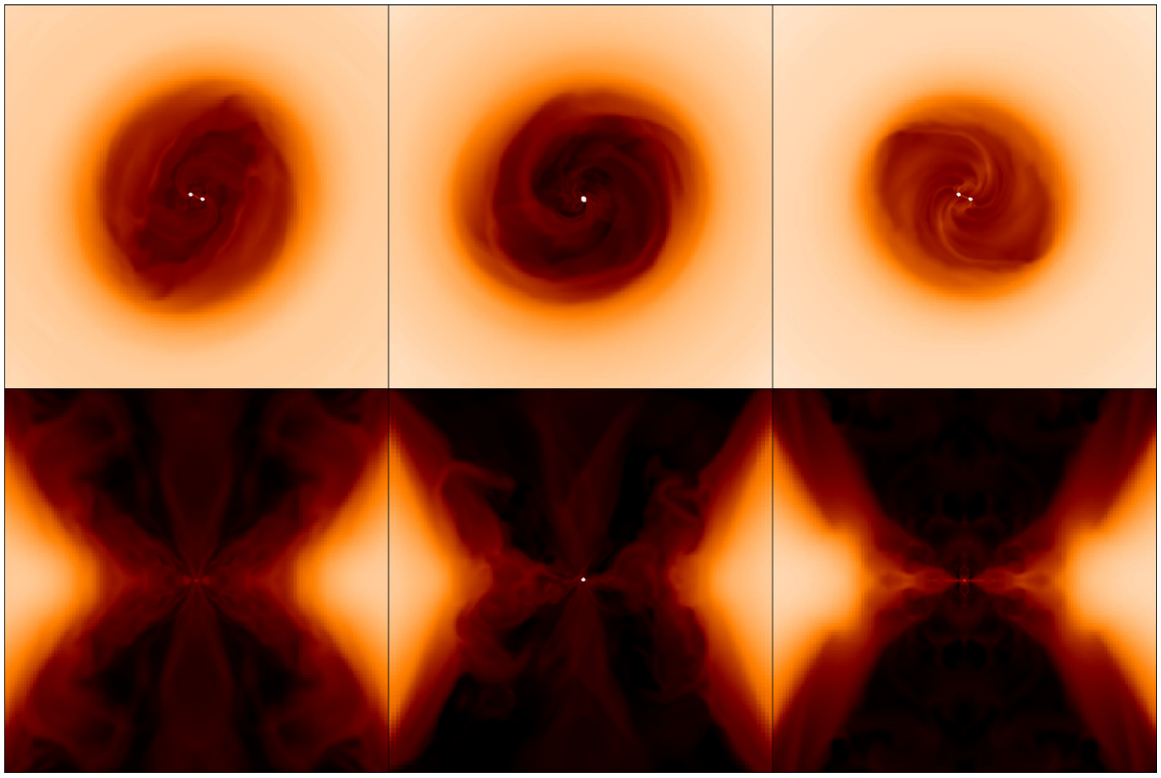

Figure 4. Density distribution of gas in circumbinary disk models DA1, DA4, and DC1, shown on a logarithmic scale, in face-on (top panels) and edge-on (bottom panels) views when the binary separation is $2\,M$. White dots mark the positions of the BHs. In panels where only one or no BHs are visible, this happens because orbital precession (top middle) or orbital motion (bottom panels) takes BHs outside of the plane of the image. Panels show a region of size $60\,M$.

(A color version of this figure is available in the online journal.)

be erased due to the emission of gravitational radiation unless there is a mechanism that can compete with it. A mechanism which has been suggested to increase the eccentricity of a BBH orbit is a resonant interaction of the binary with the circumbinary disk (Armitage & Natarajan 2005; Cuadra et al. 2009; Roedig et al. 2011). It is possible to find the radius at which the effects of gravitational radiation and the circumbinary disk are competing by setting $\dot{e}$ equal for the two cases. We adopt $\dot{e}_{\rm visc} = \mathcal{R}\,\dot{a}_{\rm visc}/2a$ and the standard expression for $\dot{e}_{\rm gw}$ (Peters 1964). Here, a is the semimajor axis of the binary and $\mathcal{R} = a\,(de/da)$ is the parameter that relates evolution of the eccentricity to that of the semimajor axis. Armitage & Natarajan (2005) compute $\mathcal{R}$ from simulations and find $\mathcal{R} \approx -0.1$ for hot disks with values of h/r comparable to those considered in this work. Assuming $h/r = 0.2$, $\alpha = 0.4$, $q = 1$, and $e = 0.8$, we find that the two effects balance each other at a binary separation of $a = 118\,M$. The assumed value of the eccentricity follows from a recent finding that binary eccentricity driven by the disk torques alone reaches a saturation value in the range 0.6–0.8 (Roedig et al. 2011). Following the GW evolution of a BBH on an eccentric orbit with $e = 0.8$ from separation $a = 118\,M$ to $8\,M$, which is a starting point of our simulations, we find that a maximal residual eccentricity is $e \approx 0.06$. The residual eccentricity only weakly depends on the binary mass ratio and has a similar value for $q = 1/2$ binary. This low residual eccentricity is insufficient for the binary to drive shocks in the distant circumbinary disk and hence, in the remainder of this paper, we focus our attention on the quasi-circular BBHs.

The parameters of the circumbinary disk models are summarized in the bottom half of Table 1. All disks are corotating with the binary except that in model DC1 which is retrograde. To minimize spurious transients caused by the initial circumbinary disk relaxing to the dynamic binary potential, the disk is "relaxed" for a period of $\sim 250\,M$. As before, we do not show this initial phase of the simulations as a part of the results reported here. In the hot accretion flow scenario this relaxation effectively eliminates spurious transients. For disks, the relaxation is not as effective and leaves behind residual slow oscillations in the bulk of the disk. These do not give rise to transients, and have little effect on the properties of the gas in the disk hole, where most of the variability is confined.

3.2. Properties of the Accretion Flow

In all simulations a plunging binary recedes promptly from the inner edge of the disk and as a consequence, the effect of the binary on the disk beyond its inner edge is relatively weak. In agreement with O'Neill et al. (2009), we do not detect shocks in the body of the disks caused by the binary motion nor by the mass loss in GWs associated with the coalescence. In the absence of characteristic variability from the body of the disk, we focus our discussion throughout the remainder of this section on the EM counterparts emanating from the disk hole.

The two BHs capture a fraction of the gas from the disk inner edge, which flows into the central region to form a low-density ambient medium surrounding the binary. Figure 4 shows the face-on and edge-on snapshots of the gas density in the central region of the DA1, DA4, and DC1 cases. Despite their differences in mass ratios and spins, the DA1 and DA4 binaries entrain a similar amount of gas from the disk. This is a combination of the two effects: while $q = 1$ on the one hand presents a larger angular momentum barrier for the inflowing gas, it also inspirals at a slower rate than a $q = 1/2$ binary, which allows it to capture gas over a longer period and somewhat offset

the primary effect. The $q = 1$ retrograde disk (DC1), on the other hand, shows a smaller central disk hole, with a higher gas density in it relative to the two previous cases. For this case, the binary and the disk interact to decrease the angular momentum of the gas, as suggested by Nixon et al. (2011), thus allowing a greater inflow rate.

To quantify the effect of the binary–disk interaction, we calculate the mean density of the gas, $\rho_{\rm h}$ in the disk hole (i.e., $R \leqslant 10\,M$) as a fraction of the disk midplane density $\rho_{\rm d}$, namely, $f_{\rm g} = \rho_{\rm h}/\rho_{\rm d}$. For $h/r = 0.2$ disks, we find $f_{\rm g} \approx 10^{-5}$, indicating the efficiency of the binary in suppressing the gas flow into the central region. For the $h/r = 0.4$ disk, $f_{\rm g} \approx 10^{-4}$, owing to the higher thermal speed of the gas which flows in at a higher rate. The orientation of spins does not seem to affect the gas inflow rate significantly.

Similar to the hot flow models the luminosity of the emerging variable EM signal will be determined by the density of the gas in the vicinity of the BBH. In our simulations the choice of h/r and α uniquely specify the gas density of the disk in hydrostatic equilibrium whose vertical structure is supported by the gas thermal pressure. It is worth noting, however, that modeling of the gas-pressure-supported disks in this work is a numerical necessity and that the innermost regions of realistic accretion disks are expected to be predominantly supported by radiation pressure (Shakura & Sunyaev 1973). A key difference between the two classes of disks is that for a given α, M, and h/r (or equivalently $\dot{M}$) the gas-pressure-supported disks are characterized by a higher gas density than radiation-pressure-supported disks. This can be intuitively understood because with the radiation as a dominant source of pressure support, disks need a smaller fraction of the thermal pressure (and hence, gas) in order to maintain the hydrostatic equilibrium. The implication is that depending on the dominant emission mechanism, the luminosity of the gas-pressure-supported disks may not trace that of the realistic disks for scenarios under consideration. We thus regard the density of the disk as a free parameter, which can be scaled to some physical value, and use $f_{\rm g}$ to estimate the fraction of the gas captured by the binary. We expect that $f_{\rm g}$ calculated from our simulations is a robust measure, regardless of the assumed structure of the disk. This is because the accretion of the gas from the inner edge of the disk (i.e., its angular momentum transport) is likely dominated by the binary torques rather than the radiation pressure or "viscous" effects. This point, however, remains to be confirmed in future simulations properly equipped to address it.

To gain context about the magnitude of the variable EM signal associated with these systems, let us consider a Shakura–Sunyaev model of a radiation-pressure-supported, steady-state disk, with $h/r = 0.2$ in the regime where Thomson scattering is the dominant source of opacity (Shakura & Sunyaev 1973). Using maximum radiative efficiency for the Schwarzschild BH, one finds at the disk inner edge a temperature 2.5×10^5 K and $\rho_{\rm d} \approx 3.5 \times 10^{-11}\,{\rm g\,cm^{-3}}$. Since in the central region $f_{\rm g} \sim 10^{-5}$ and the gas is promptly shock-heated to $T_p \sim 10^{11}$ K, the disk hole acquires the properties of the hot accretion flow discussed in the previous section. Assuming that in this case $\varepsilon = T_e/T_p = 0.1$, the upper limit on the bremsstrahlung luminosity from the disk hole and Bondi accretion rate onto the BHs are

$$L_{\rm brem} \approx 1.6 \times 10^{35}\,{\rm erg\,s^{-1}}\,\varepsilon_{-1}^{1/2}\,f_{\rm g,-5}^2\,\rho_{\rm d}'^2\,R_{10}^3\,T_{p,11}^{1/2} \times (1 + 4.4\,\varepsilon_{-1}\,T_{p,11})_{5.4}\,M_7^3\,, \quad (5)$$

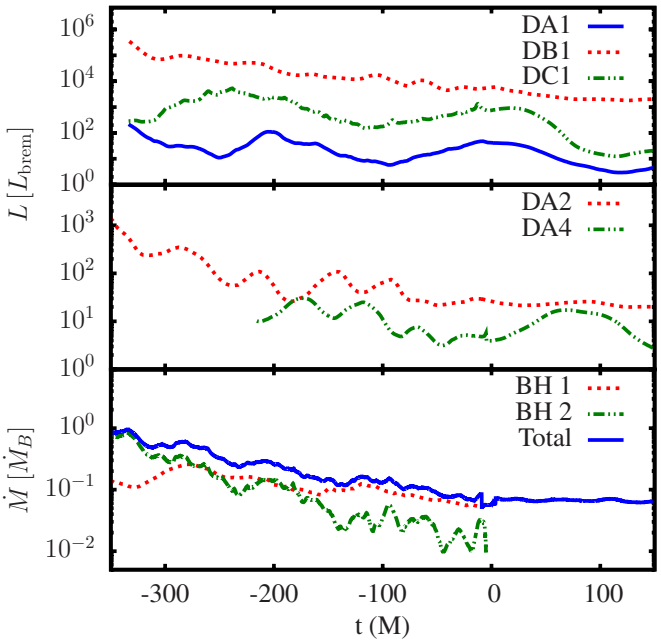

Figure 5. Bremsstrahlung luminosity from the disk hole (top two panels) in units of $L_{\rm brem}$ given by Equation (5). Total and individual BH accretion rates for the case DA2 (bottom panel) in units of $\dot{M}_B$ given by Equation (6).

(A color version of this figure is available in the online journal.)

$$\dot{M}_{\rm B} \approx 2.5 \times 10^{-4}\,M_\odot\,{\rm yr^{-1}}\,f_{\rm g,-5}\,\rho_{\rm d}'\,T_{p,11}^{-3/2}\,M_7^2\,. \quad (6)$$

If a strong magnetic field is present, assuming $\beta = 10$,

$$L_{\rm syn} \approx 2.5 \times 10^{36}\,{\rm erg\,s^{-1}}\,\beta_{10}^{-1}\,f_{\rm g,-5}^2\,\rho_{\rm d}'^2\,R_{10}^3\,T_{p,11}\,M_7^3\,, \quad (7)$$

where $\varepsilon = 0.1\varepsilon_{-1}$, $f_{\rm g} = 10^{-5}\,f_{\rm g,-5}$, $\rho_{\rm d}' = \rho_{\rm d}/3.5 \times 10^{-11}\,{\rm g\,cm^{-3}}$, $R = 10M\,R_{10}$, and $T_p = 10^{11}\,{\rm K}\,T_{p,11}$. While higher than the bremsstrahlung, the synchrotron luminosity is still modest in absolute terms for $M \leqslant 10^7\,M_\odot$ BBH systems. As in the case of a hot accretion flow, it can be shown here that the inverse Compton luminosity can be of order of $L_{\rm syn}$ and $L_{\rm brem}$. In this case, however, the shocked gas from the central low-density region can more easily (adiabatically) expand into the ambient medium. As a consequence, the temperature of the gas remains below the 100 MeV threshold for π^0 production in most of the computational volume and the emission of γ-ray photons due to pion decay is expected to be inefficient.

Figure 5 shows the bremsstrahlung light curves integrated within a sphere of radius $R = 10\,M$, ensuring contribution only from the diffuse gas in the disk hole. The top panel shows the $q = 1$ cases. The long period variations in the luminosity in $h/r = 0.2$ models (DA1 and DC1) correspond precisely to the orbital frequency at radius $R = 10\,M$ and arise due to the flow of gas streams on eccentric orbits in and out of the integration domain. This is evident in the first and third panels of Figure 4, which illustrate that the distribution of gas in the vicinity of $q = 1$ binaries is ellipsoidal due to the binary torques. The formation of the eccentric streams of matter in response to the BBH torques is a salient property of binary–circumbinary disk systems and has previously been pointed out in the context of Newtonian simulations (Hayasaki et al. 2007; MacFadyen & Milosavljević 2008; Cuadra et al. 2009). This type of variation is not observed in the "hotter" $h/r = 0.4$ disk (DB1). In this case the binary is less efficient at driving a resonant motion

of the surrounding gas and it finds itself immersed into a relatively uniform density medium. The decrease in the overall luminosity in these three cases is consistent with the scaling $L_{\rm brem} \propto f_{\rm g}^2$ implied by Equation (5). The accretion rates reflect a similar behavior, namely, the scaling $\dot{M}_{\rm B} \propto f_{\rm g}$ from Equation (6).

The middle panel in Figure 5 shows light curves from the $q = 1/2$ binaries (DA2 and DA4). The binaries in these cases induce a more circularly symmetric distribution of gas within the disk hole (see DA4 case in Figure 4). The variability or oscillations in the light curves are, unlike for $q = 1$ binaries, associated with the orbiting wakes following the BHs and thus follow the BBH orbital motion. Notice also that here again the luminosity of the misaligned spins case (DA4) falls below its counterpart with parallel spins (DA2). However, unlike the case of the hot accretion flows there is no pre-merger flare and subsequent drop-off in luminosity at merger. The lack of these two signatures in the disk scenario can be attributed to the contrasting density distributions in the two scenarios: in the hot flow the gas density increases toward the center of the binary potential while in the circumbinary disk case the density is lowest at the center of the system, as illustrated in the bottom panels of Figure 4. This occurs because the gas is only slowly "leaking" from the inner edge of the disk into the central region. The luminosity of a dilute gas powered by shocks from the BBH motion just before the merger is overtaken by the luminosity of the remainder of the gas in the disk hole. Consequently, the luminosity peak associated with the BBH merger is invisible in the light curves shown in the top panels of Figure 5.

The bottom panel in Figure 5 shows the accretion rates onto the primary and secondary BHs, as well as the total, in model DA2. Note that initially the accretion rate onto the lower mass secondary BH exceeds that of the primary because it orbits closer to the inner edge of the disk where it captures and accretes gas (Artymowicz & Lubow 1996; Gould & Rix 2000). Later in the inspiral, the primary increasingly captures gas bound to the secondary and augments its accretion rate until time $\approx -250M$ before merger, when the accretion rates of the primary and secondary are reversed and the primary becomes the dominant accretor.

Our simulations indicate that low-luminosity variability described in this section would be challenging to detect in observational campaigns searching for BBHs, except perhaps for massive systems with $M \gg 10^7\,M_\odot$. The situation is more severe for "thinner" disks in which the central regions are expected to be even less luminous. In these disks, the radial inflow velocity at the inner edge is $\propto (h/r)^2$, resulting in the decoupling of the binary from the disk even earlier in the inspiral. As a consequence, the gas in the disk hole will have lower density and thus be even dimmer. The circumbinary disk itself will likely overwhelm the overall emission and shield any sign of variability from the disk hole although, strictly speaking, the light emitted by the disk is expected to peak in the optical and UV-band, while the bremsstrahlung and inverse Compton emission from the $T_p \sim 10^{11}$ K gas in the hole is expected to peak at $\sim$100 keV. Because of its radiatively inefficient nature the gas in the disk hole would exhibit similar emission properties to the hot flow described in Section 2.2.

4. CONCLUSIONS

We studied the EM signatures associated with the late inspiral and merger of supermassive BBHs with unequal masses, different BH spin orientations, and two environments (hot accretion flows and circumbinary disks).

In a *hot accretion flow*, the plunge and merger of the binary give rise to a characteristic flare followed by a sudden drop-off. This and earlier hydrodynamic simulations (Bode et al. 2010; Farris et al. 2010) indicate that the flare is a robust signature that arises in all modeled BBH configurations and hot accretion flows regardless of the specific setup of initial conditions. The amplitude of the flare and the drop-off are more pronounced in lower temperature flows, where shocking is more predominant. We find that the shape and amplitude of the flare depend on a mass ratio and spin configuration to a lesser degree. A hot flow is also characterized by quasi-periodic variability from the beaming of light emitted by the gas wakes behind the BHs. In all cases, this EM equivalent of a "chirp" is directly mirrored by the GWs (the existence of such signature has previously been predicted by Kocsis et al. 2008). If observed, either signature (flare or variability) would be a smoking gun for an impending BBH coalescence in a hot accretion flow environment.

In the *circumbinary disk* case we modeled geometrically thick disks characterized by high radial inflow velocities, which can follow the binary until late in the GW-driven inspiral. We find that a combination of the properties of such disks and the prompt decoupling of the binary from their inner edge result in an absence of shocks and luminous EM flares from the body of the disks. The only region where variable EM signatures emerge is the central low-density hole surrounding the binary. We find that the gas in this central region also has the properties of an RIAF. In unequal-mass BBH systems, its luminosity exhibits variability related to the BBH orbital dynamics. In equal-mass systems, however, the variability traces the dynamics of the gas streams plunging from the inner edge of the disk and is not correlated with the frequency of GWs. In all cases, the emission from the central region is low and based on our models, unlikely to be observed for BBH systems $\leqslant 10^7\,M_\odot$.

In summary, while BBH mergers in both the hot accretion flows and circumbinary disks exhibit characteristic EM signatures, we find that the former is more likely to be sufficiently luminous to be observed. To be observable, any variability must be more pronounced than the natural variability of "normal" AGNs. While the flare signaling the merger seems to satisfy this condition, the quasi-periodic oscillations will be more challenging to observe. A precursor GW detection by a space interferometer could in principle alert EM observatories in advance, and hopefully alleviate this challenge.

An interesting question is whether, in the absence of a GW precursor, the flares and variability can be detected in standalone EM observations. Given that more massive BBH systems are also expected to be more luminous, a future serendipitous discovery of $\gtrsim 10^8\,M_\odot$ BBH coalescence by a burst alert mission cannot be excluded. A more systematic search will require deep monitoring of the transient sky with multiwavelength synoptic sky surveys. While this biases EM searches toward the high BH masses, they are complimentary to future GW observations that will likely be optimized to search for the lower mass end supermassive BBHs. Both will be required in order to eventually understand the properties of the BBH population and their role in the evolution of galaxies and structure in the universe.

We thank the anonymous referee for thoughtful comments which helped to improve this manuscript. T. Bogdanović is supported by a NASA Einstein Postdoctoral Fellowship Award

PF9-00061 from the *Chandra X-ray Observatory* Center operated by Smithsonian Astrophysical Observatory for and on behalf of NASA contract NAS8-03060. This work is supported by NSF grants 0653443, 0855892, 0914553, 0941417, 0903973, and 0955825. Computations were carried out under Teragrid TG-MCA08X009 and at the Georgia Tech FoRCE cluster.

REFERENCES

Ansorg, M., Brügmann, B., & Tichy, W. 2004, Phys. Rev. D, 70, 064011
Armitage, P. J., & Natarajan, P. 2002, ApJ, 567, L9
Armitage, P. J., & Natarajan, P. 2005, ApJ, 634, 921
Artymowicz, P., & Lubow, S. H. 1994, ApJ, 421, 651
Artymowicz, P., & Lubow, S. H. 1996, ApJ, 467, L77
Baiotti, L., Hawke, I., Montero, P. J., et al. 2005, Phys. Rev. D, 71, 024035
Bhattacharyya, S., Bhatt, N., & Misra, R. 2006, MNRAS, 371, 245
Bode, T., Haas, R., Bogdanović, T., Laguna, P., & Shoemaker, D. 2010, ApJ, 715, 1117
Bogdanović, T., Smith, B. D., Sigurdsson, S., & Eracleous, M. 2008, ApJS, 174, 455
Cactus 2010, Cactus Computational Toolkit, http://cactuscode.org
Cao, X. 2011, ApJ, 737, 94
Colpi, M., Dotti, M., Mayer, L., & Kazantzidis, S. 2007, in 2007 STScI Spring Symp.: Black Holes, ed. M. Livio & A. M. Koekemoer (Cambridge: Cambridge Univ. Press)
Colpi, M., Maraschi, L., & Treves, A. 1986, ApJ, 311, 150
Cuadra, J., Armitage, P. J., Alexander, R. D., & Begelman, M. C. 2009, MNRAS, 393, 1423
Dahlbacka, G. H., Chapline, G. F., & Weaver, T. A. 1974, Nature, 250, 36
Dotti, M., Salvaterra, R., Sesana, A., Colpi, M., & Haardt, F. 2006, MNRAS, 372, 869
Eilek, J. A., & Kafatos, M. 1983, ApJ, 271, 804
Einstein Toolkit 2010, Einstein Toolkit: Open Source for Relativistic Astrophysics, http://einsteintoolkit.org
Farris, B. D., Liu, Y. T., & Shapiro, S. L. 2010, Phys. Rev. D, 81, 084008
Gould, A., & Rix, H. 2000, ApJ, 532, L29
Hayasaki, K., Mineshige, S., & Sudou, H. 2007, PASJ, 59, 427
Ho, L. C. 2005, Ap&SS, 300, 219
Husa, S., Hinder, I., & Lechner, C. 2006, Comput. Phys. Commun., 174, 983
Ichimaru, S. 1977, ApJ, 214, 840
Klein, A., Jetzer, P., & Sereno, M. 2009, Phys. Rev. D, 80, 064027
Kocsis, B., Haiman, Z., & Menou, K. 2008, ApJ, 684, 870
MacFadyen, A. I., & Milosavljević, M. 2008, ApJ, 672, 83
Mahadevan, R., Narayan, R., & Krolik, J. 1997, ApJ, 486, 268
Milosavljević, M., & Phinney, E. S. 2005, ApJ, 622, L93
Mösta, P., Palenzuela, C., Rezzolla, L., et al. 2010, Phys. Rev. D, 81, 064017
Narayan, R., & Yi, I. 1994, ApJ, 428, L13
Nemmen, R. S., Storchi-Bergmann, T., Yuan, F., et al. 2006, ApJ, 643, 652
Nixon, C. J., Cossins, P. J., King, A. R., & Pringle, J. E. 2011, MNRAS, 412, 1591
Oka, K., & Manmoto, T. 2003, MNRAS, 340, 543
O'Neill, S. M., Miller, M. C., Bogdanović, T., Reynolds, C. S., & Schnittman, J. D. 2009, ApJ, 700, 859
Palenzuela, C., Anderson, M., Lehner, L., Liebling, S. L., & Neilsen, D. 2009, Phys. Rev. Lett., 103, 081101
Palenzuela, C., Lehner, L., & Liebling, S. L. 2010, Science, 329, 927
Peters, P. C. 1964, Phys. Rev., 136, 4B
Roedig, C., Dotti, M., Sesana, A., Cuadra, J., & Colpi, M. 2011, MNRAS, 415, 3033
Schnetter, E., Hawley, S. H., & Hawke, I. 2004, Class. Quantum Grav., 21, 1465
Shakura, N. I., & Sunyaev, R. A. 1973, A&A, 24, 337
Sharma, P., Quataert, E., Hammett, G. W., & Stone, J. M. 2007, ApJ, 667, 714
Thornburg, J. 2004, Class. Quantum Grav., 21, 743
Trias, M., & Sintes, A. M. 2008, Phys. Rev. D, 77, 024030
van Meter, J. R., Wise, J. H., Miller, M. C., et al. 2010, ApJ, 711, L89